

# Reinforcement Learning for Adaptive Composition of Quantum Circuit Optimisation Passes

Daniel Mills<sup>1</sup>, Ifan Williams<sup>1</sup>, Jacob Swain<sup>2</sup>, Gabriel Matos<sup>2</sup>, Enrico Rinaldi<sup>2</sup>, and Alexander Koziell-Pipe<sup>2</sup>

<sup>1</sup>Quantinuum, Terrington House, 13–15 Hills Road, Cambridge CB2 1NL, United Kingdom

<sup>2</sup>Quantinuum, Partnership House, Carlisle Place, London SW1P 1BX, United Kingdom

## Abstract

Many quantum software development kits provide a suite of circuit optimisation passes. These passes have been highly optimised and tested in isolation. However, the order in which they are applied is left to the user, or else defined in general-purpose default pass sequences. While general-purpose sequences miss opportunities for optimisation which are particular to individual circuits, designing pass sequences bespoke to particular circuits requires exceptional knowledge about quantum circuit design and optimisation. Here we propose and demonstrate training a reinforcement learning agent to compose optimisation-pass sequences. In particular the agent’s action space consists of passes for two-qubit gate count reduction used in default PyTKET pass sequences. For the circuits in our diverse test set, the (mean, median) fraction of two-qubit gates removed by the agent is (57.7%, 56.7%), compared to (41.8%, 50.0%) for the next best default pass sequence.

## 1 Introduction

Quantum circuit optimisation transforms a quantum circuit to improve the quality of its output. This quality can, for example, be measured by the fidelity of the output state to the ideal output state, or the accuracy of some derived quantity such as an observable expectation value. Often the number of two-qubit gates in the circuit is the dominant noise source [1], and so can be used as a proxy for the total noise affecting the circuit. In such cases, to increase the quality of a circuit’s output it is desirable to reduce the number of two-qubit gates.

*Optimisation passes* for reducing two-qubit gate count are the most relevant for existing devices, and as such are abundant and readily available in popular quantum software development kits (QSDKs) [2–9]. Examples include passes for Clifford subcircuit optimisation [10], uni-

tary resynthesis [4], ZX-calculus-based rewriting [7], and Pauli-gadget-based optimisation [8]. Many QSDKs offer default heuristic based sequences of optimisation passes, constructed to perform well in the typical case.

There are however at least two obstacles to the widespread effective utilisation of optimisation passes. Firstly, optimisation passes regularly target particular circuit structures or employ advanced circuit rewriting techniques. As such, recognising when an optimisation pass can be beneficially applied often requires extraordinary expertise in circuit construction and optimisation. Secondly, selecting a sequence of optimisations is susceptible to the *Phase Ordering Problem* [11], wherein the order of application of optimisations can impact the quality of the resulting circuit. Again, this can be hard to account for without very careful study of the particular circuit of concern. For the above reasons, fixed default pass sequences cannot be optimal in all cases, and a sequence bespoke to the circuit is preferred.

Here we resolve this by using reinforcement learning (RL) to train an agent to analyse a quantum circuit, and propose a bespoke sequence of optimisation passes. We use Proximal Policy Optimisation (PPO) [12] with graph neural network (GNN) layers [13, 14], leveraging the native graph structure of quantum circuits. The model draws actions from a set of existing optimisation passes, improving on the utilisation of already available techniques. In particular, we demonstrate that when our model chooses from a selection of PyTKET [2] passes it outperforms default sequences of optimisation passes provided by PyTKET. On our comprehensive test set, the (mean, median) fraction of initial two-qubit gates removed by the agent is (57.7%, 56.7%), compared to (41.8%, 50.0%) for the next best PyTKET default pass sequence. Finally, we compare our model to search-based approaches, which also create circuit-bespoke pass sequences. We demonstrate that our model produces optimised circuits of comparable two-qubit gate count to these search-based approaches, but at a notably lower

time cost at execution.

## 2 Related Work

Quetschlich et al. [15–17] consider the related problem of selecting the device and the default optimisation-pass sequence best suited for a particular circuit. Here we focus on outperforming the default passes and fix the device. Further, the choice of neural network architecture used in Quetschlich et al. [15–17] limits the agent to inputs from a fixed-size observation space consisting of a fixed number of features of the circuit. The agent introduced in this work takes the whole circuit as input, with no limit to the size of the circuit imposed by the model architecture, so it is not limited to making predictions based on only a few features. Dangwal et al. [18] also consider optimisation-pass selection but, rather than using neural networks, rely on classical simulation to rank optimisation passes. Clifford circuits similar to the original circuit, rather than the original circuit itself, are optimised and used to predict the performance of optimisation passes on the original circuit. Not using the original circuit limits the accuracy of the predictions, which is why we do use the original circuit here.

This work sets out to improve the utilisation of existing *global* optimisation passes; those which rewrite the entirety of – or large parts of – a circuit at once. We consider global passes as they are the most abundant and well developed, and have been composed into the most carefully considered baseline default pass sequences. However, other works have used machine learning (ML) to support *local* rewriting. Fösel et al. [19] employ convolutional neural networks acting on 3D grid representations of quantum circuits. The trained RL agent selects simple local rewrites, such as gate commutation and cancellation, on circuits with nearest neighbour connectivity. Li et al. [20] utilise learned local representations of gates in a circuit to select a location in a circuit and a local transform to apply at that location, introducing a splitting of the action space to reduce its dimension. Neural network architectures have also been employed to select more complex local transformations based on the ZX calculus [21–24]. Relatedly, Xu et al. [25] and Xu et al. [26] perform a greedy search over local rewrites.

Besides two-qubit gate count optimisation, Ruiz et al. [27] consider T-gate count reduction; translating circuits into a 3D “signature tensor” and utilising an extension of the AlphaTensor [28] transformer-based model to optimise portions of a circuit. Other works have considered the problems of *routing* and *circuit layout*, which take into account the constraints inherent to the connectivity of underlying hardware architecture. These works use techniques such as Monte-Carlo tree search [29, 30] and

RL [31–34]. As well as optimising existing circuits, ML has also been employed for the purpose of *circuit synthesis* [35–39], where a target state or unitary is given and a new circuit implementing it must be constructed. It has also been employed to search for variational quantum algorithm ansatzes [40].

## 3 RL for Pass Sequence Selection

In this work, we train an RL agent to, given a quantum circuit, iteratively select and apply a sequence of optimisation passes. The circuit is first encoded in a graph. PPO is used to train an actor-critic pair of GNNs to produce the best next pass in the sequence. Figure 1 gives an overview of our method, which we describe in detail below.

### 3.1 Graph representation of circuits

Our graph encoding of the circuit uses nodes to represent gates, qubit inputs, and qubit outputs. Qubits are represented by edges, which give the order in which gates are applied to a given qubit. This allows for a natural representation of circuits with arbitrary connectivity, unlike 3D tensor representations of circuits. An example of the graph representation is given in Fig. 2.

Here we will use circuits in the universal *Quantinuum native gateset*: ZZPhase, Rz, PhasedX [1]

$$\text{ZZPhase}(\alpha) = e^{-\frac{1}{2}i\pi\alpha Z \otimes Z}, \quad (1)$$

$$\text{Rz}(\alpha) = e^{-\frac{1}{2}i\pi\alpha Z}, \quad (2)$$

$$\text{PhasedX}(\alpha, \beta) = \text{Rz}(\beta) \text{Rx}(\alpha) \text{Rz}(-\beta), \quad (3)$$

where  $\text{Rx}(\alpha) = e^{-\frac{1}{2}i\pi\alpha X}$ . Each node is represented by an 8-element feature vector consisting of: a boolean flag indicating if the node is an input; a boolean flag indicating if the node is an output; the normalised Rz gate parameter; the set of normalised PhasedX gate parameters; the normalised ZZPhase gate parameter; a boolean flag indicating if the gate is a Clifford gate; and an index of the most recent optimisation pass that was applied to the circuit, or -1 if no pass has been applied. Only one of the three gate parameters can be non-zero, ensuring the node corresponds uniquely to a gate. Similarly a node cannot be a gate and an input/output, nor can a node be an input and an output.

The Clifford-gate flag is included to mitigate a representation issue with neural networks caused by Clifford angles being arbitrarily close to non-Clifford angles. The index of the most recent optimisation pass is included to avoid repetition of idempotent optimisation passes.

Edges have a source and a destination node. In the context of each node, the qubit corresponding to the edge

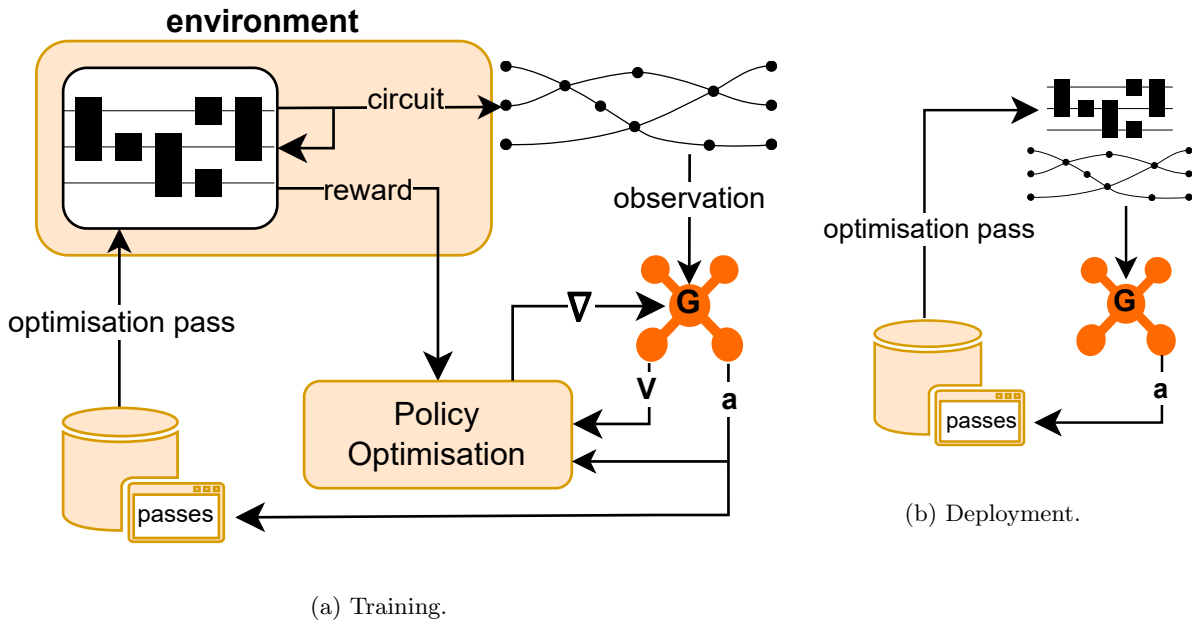
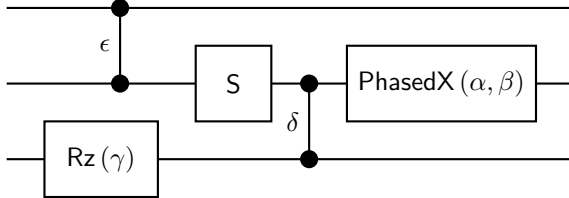
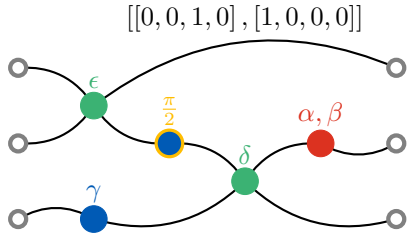


Figure 1: **Training and deploying an RL agent for optimisation-pass selection as described in this work.**  
a: A quantum circuit is loaded into the environment and transformed into a graph representation, as discussed in Section 3.1. This graph (the RL “observation” [41]) is processed by a pair of GNNs,  $\mathbf{G}$ , as discussed in Section 3.3. The actor network outputs a vector of logits,  $\mathbf{a}$ , for selecting the next optimisation pass; the critic head estimates the current circuit state value,  $\mathbf{V}$ . An optimisation pass, as discussed in Section 3.2, is selected via softmax sampling of  $\mathbf{a}$  and applied to the circuit. The reward, along with  $\mathbf{V}$  and  $\mathbf{a}$ , is used to compute gradients,  $\nabla$ , and update  $\mathbf{G}$  via PPO. The environment is reset with a fresh circuit from the training dataset (discussed in Section 3.4) whenever either: the DoNothing pass is selected; the two-qubit gate count is reduced to 0; or a preset number of passes are applied with no observed improvement.

b: An input circuit is converted to a graph and repeatedly ingested by the actor network of  $\mathbf{G}$ . Optimisation passes are selected via argmax sampling of  $\mathbf{a}$ . The cycle terminates when the DoNothing pass is selected, and the optimised circuit is returned to the user.



(a) An example circuit, comprising of  $Rz$ ,  $PhasedX$ , and  $ZZPhase$  gates.  $ZZPhase$  gates are represented by black dots connected by vertical lines, with Greek letters (in this case  $\delta$  and  $\epsilon$ ) giving the associated gate angle.



(b) The circuit graph of a. Colours correspond to gate type (green =  $ZZPhase$ , blue =  $Rz$ , red =  $PhasedX$ ), with a yellow ring depicting the additional flag in the case of Clifford gates. Inputs and outputs are grey. An example edge encoding is given for the neighbouring edge, which corresponds to  $[[0, 0, 1, 0], [1, 0, 0, 0]]$  because the source node of the edge corresponds to the ‘first’ qubit acted on by the  $ZZPhase$  gate, and the destination node corresponds to an output.

Figure 2: Example circuit encoded as a graph.

can be either: an input/output qubit; the target of a single-qubit gate; the ‘first’ qubit acted on by a two-qubit gate; or the ‘second’ qubit acted on by a two-qubit gate.<sup>12</sup> As such, the source and destination can each be described by a length-4 one-hot encoding, giving a length-8 vector for each edge. We use the above order of features in the example edge encoding of Fig. 2b.

## 3.2 Action Space

The agent’s action space consists of the following optimisation passes:

**KAKDecomposition:** Find and optimally resynthesise two-qubit subcircuits [42].

**CliffordResynthesis:** Find and resynthesise Clifford subcircuits [43].

<sup>1</sup> $ZZPhase$  is symmetric so does not have a fundamental notion of ‘first’ and ‘second’. Instead we assign these labels to qubits arbitrarily.

<sup>2</sup>Qubits are labelled as ‘first’ and ‘second’ in order to match input wires of the node to output wires when they concern the same qubit.

**CliffordSimp:** Apply rewrite rules simplifying Clifford gate sequences according to Fagan et al. [10].

**ZXGraphlikeOptimisation:** Simplify circuit in ZX-calculus and extract circuit from simplified diagram according to Backens et al. [44].

**GreedyPauliSimp:** Convert a circuit into a graph of Pauli gadgets and resynthesise according to Paykin et al. [8] and Schmitz et al. [45].

**ThreeQubitSquash:** Find and resynthesise three-qubit subcircuits [46].

**DoNothing:** Do not alter the circuit and terminate.

Besides **DoNothing**, these passes are built from passes in PyTKET (version 2.9.3) with the same name. As the output gateset used by each PyTKET pass is different, after the application of each pass the circuit is also rebased to the Quantinuum native gateset.

## 3.3 Training Methodology

We use a GNN to compute a learned representation of the nodes of the graph. We use graph convolutional layers to ensure the receptive field of the graph nodes encompasses a large enough neighbourhood to capture discriminative features. To incorporate edge features, we use the modified GINConv operator of Hu et al. [47]. We use skip connections to avoid vanishing gradients and improve information flow [48]. We use mean pooling to construct a graph-level representation vector, ensuring that the trained network can ingest circuits of different sizes. A simple feed-forward network is used to compute action logits and state values from the graph-level representation. In our PPO implementation, gradient updates are performed using the Adam optimiser [49].

Let a circuit have  $n_0$  two-qubit gates before any optimisation has taken place. After the application of  $t$  optimisation passes it has  $n_t$  two-qubit gates. The reward for the  $t^{\text{th}}$  action is

$$r_t = \frac{n_{t-1} - n_t}{n_0}. \quad (4)$$

We will use *reward* to refer to the reward from the application of a single optimisation pass. We will use *cumulative reward* to refer to the total reward received by a sequence of optimisation passes; i.e.  $\sum_t r_t$ . The cumulative reward can be interpreted as the fraction of two-qubit gates removed by a pass sequence.

The normalisation by the denominator in Eq. (4) guarantees that the maximum attainable cumulative reward for any circuit is 1.0. This ensures equal consideration of large and small circuits. During training, to encourage efficient use of optimisation passes, we additionally

Parameter	Value
<b>PPO</b>	
Learning rate	$3.36 \times 10^{-4}$
Number of steps	128
Batch size	64
Number of epochs	3
Discount factor ( $\gamma$ )	0.952
GAE( $\lambda$ )	0.938
Clip range	0.2
Entropy coefficient	0.01
Value function coefficient	0.5
Gradient clipping maximum value	0.5
Action penalty	0.013
<b>GNN Architecture</b>	
Number of convolutional layers	4
Hidden layer dimension	128

Table 1: Optimised hyperparameters for the PPO and GNN architecture.

include a small penalty for taking an action other than `DoNothing`.

The hyperparameters of the PPO algorithm and the specific architecture of the GNN are selected via hyperparameter optimisation. Trial parameters are sampled based on the Tree-structured Parzen Estimator algorithm [50]. An initial search over the most influential parameters is carried out over 50 trials. For the PPO, these are: the learning rate, the action penalty,<sup>3</sup> the batch size, the number of training epochs, and the number of training steps per update. For the GNN, these are the number of graph convolutional layers and the hidden layer dimension. Following this, a second search over 50 trials is carried out, where the optimal parameters from the initial search are fixed, and some additional PPO hyperparameters of secondary influence are scanned. These are the discount factor,  $\gamma$ , and the Generalised Advantage Estimation bias-variance trade-off factor, GAE( $\lambda$ ). All hyperparameters, including those not covered by the search, are given in Table 1.

### 3.4 Datasets

Training and testing is performed with synthetic circuits, randomly generated from the following circuit classes:

**Random-SU4:** Random SU(4) gates acting on random

<sup>3</sup>In practice the action penalty could be set according to the trade-off between the cost of spending time and compute resources on circuit optimisation versus the benefit gained from removing two-qubit gates. In the absence of a well-defined metric for this trade-off, we model the action penalty as a hyperparameter and determine its value through hyperparameter optimisation.

qubit pairs. Inspired by quantum volume circuits [51].

**Random-SU8:** Random SU(8) gates acting on random triples of qubits.

**IQP:** Random sequences of commuting gates [52], commonly used as variational ansatzes [53, 54].

**QAOA:** Random instances of a popular ansatz used for optimisation problems [55].

**Pauli:** Random sequences of Pauli gadgets [56].

**Clifford-SU4:** Circuits composed of a mixture of random Clifford subcircuits and random SU(4) gates.

**Ordered-Clifford-SU4:** Constructed by sandwiching random Clifford identities between sets of random two-qubit gates.

**Clifford-SU4-SU8:** Circuits composed of a mixture of random Clifford subcircuits, random SU(4) gates, and random SU(8) gates.

These circuits are a mixture of application motivated circuits, and circuits constructed to expose the model to complex structures. These circuits are expected to require relatively short sequences of the actions listed in Section 3.2,<sup>4</sup> but recognising the correct sequence by eye is challenging and time consuming. We minimally preprocess the circuits so that they are in the Quantum default gateset. To thoroughly test the optimisation methods, we do not assume that any prior optimisation has occurred. We do not impose any connectivity restrictions on the circuits we generate, which is naturally supported by our use of GNNs.

The training set comprises 402,558 circuits, of which 10% are withheld for validation. Circuits are of a range of sizes, with qubit counts spanning the range [3, 7], and two-qubit gate counts spanning the range [0, 215].<sup>5</sup>

### 3.5 Training and Deployment

The model is trained using PPO as implemented in Stable Baselines3 [41] (version 2.7.1), employing vectorised execution over 8 parallel environment instances. Experiments are conducted on a Lightning-AI-hosted [57] machine equipped with a single NVIDIA L4 Tensor Core GPU, 16 vCPUs, and 64 GB of RAM. Evaluation is also performed on the same machine, unless otherwise stated.

<sup>4</sup>Circuits requiring long sequences of passes are rare. This is in part because global optimisation passes often conflict with each other when run in sequence. This is an important aspect of the Phase Ordering Problem, and is discussed further in Section 5.

<sup>5</sup>For circuits generated with no two-qubit gates, the model performs no optimisation and simply returns the original circuit, giving a total reward of 0.

Training is limited to a maximum number of steps (application of passes) of 300,000, with early stopping triggered when the performance on validation data has stagnated. As an example, in practice this early stopping occurred (for one particular training seed) after 147,500 steps, corresponding to a wall-clock training time of 2.73 hours.

Once the model has been trained, the actor network can be easily deployed. An input circuit, represented in graph form, is ingested by the network, which selects the next pass which is then applied to the circuit. This process is repeated until one of the following occurs: the two-qubit gate count is 0; the `DoNothing` action is selected; a fixed number (configurable) of passes has been applied with no further reduction in two-qubit gate count. At this point, the optimised circuit is returned to the user.

## 4 Results

Here we present results comparing our trained model to the following default PyTKET (version 2.9.3) optimisation-pass sequences:

**FullPeepholeOptimise:** A general-purpose sequence of passes performing a combination of two- and three-qubit subcircuit squashing, and Clifford circuit simplification.

**QuantinuumDefaultTwo:** Similar to `FullPeepholeOptimise`, but optimised for the Quantinuum H-series devices.

**QuantinuumDefaultThree:** Similar to `GreedyPauliSimp`, but optimised for the Quantinuum H-series devices.

`FullPeepholeOptimise` is derived from a PyTKET pass of the same name. The latter two passes are default optimisation passes for the PyTKET Quantinuum backend (optimisation levels set as in the pass name [58]). Note that `QuantinuumDefaultTwo`, `QuantinuumDefaultThree`, and `FullPeepholeOptimise` are built from several individual passes [2, 58]. We additionally compare to `GreedyPauliSimp` and `KAKDecomposition`, as these are particularly performant single passes.

**In-Distribution Testing** Results in Fig. 3 report performance on a test dataset consisting of 40,412 circuits, approximately equally distributed across circuit classes. These circuits are unseen during training, but are drawn from the same distribution as those in the training set; hence referred to as ‘in-distribution’ circuits. The model is trained 9 times, each time with a different initial seed (weights initialisation), to give an agent for each seed.<sup>6</sup>

<sup>6</sup>Due to stochastic training, performance varies across random seeds. We report statistics over multiple independently trained

Each circuit is optimised once with each agent. The baseline optimisation passes are deterministic, therefore each circuit is optimised only once per baseline optimisation pass. As such, in total there are  $40,412 \times (9+5) = 565,768$  optimised circuits; 40,412 for each baseline default pass, and 363,708 for the ‘RL Model’. The box plots in Fig. 3 give the distribution, over optimised circuits, of the cumulative reward.

The median cumulative rewards over all circuits (‘Full test dataset’ in Fig. 3) are 0.567 and 0.500 for the model and the best PyTKET default pass respectively (`QuantinuumDefaultTwo`). Further, the distribution of cumulative reward for the model is skewed upwards as compared to the other passes. This is reflected in the notable improvement in mean cumulative reward: 0.577 for the model, compared to 0.418 for `QuantinuumDefaultTwo`. This demonstrates that while the default passes are typically good, a bespoke approach is preferred in many cases. In particular, most default passes have a circuit class or two where they perform particularly poorly. Conversely, for the majority of circuit classes the model generates the sequence of passes with the highest – or close to the highest – median cumulative reward of all the passes compared.

Figure 4 gives the distributions, over optimised circuits, of the difference between the model’s cumulative reward and the cumulative reward of the baseline methods. This shows that the median performance of the model is always as good as – or better than – the baseline methods. We also see that for the Clifford-SU4-SU8, Clifford-SU4, and Ordered-SU4-SU4 circuit classes, the median performance is always better than even the best baseline method. This again demonstrates that the model does more than simply reproduce the best baseline approach.

It is important to note that the agent is indeed generating a bespoke sequence of passes for each circuit, rather than, say, simply applying all passes repeatedly. This is important for the usability of the trained agent, as the time taken to execute excessively long sequences of passes would be very costly. For example, the model performs identically to the `GreedyPauliSimp` in the case of IQP and Pauli circuits. This is because just a single pass is best in this case, with the agent performing a one-pass sequence consisting only of `GreedyPauliSimp` in  $\sim 99.6\%$  and  $\sim 99.1\%$  of cases, respectively. In the case of Clifford-SU4 and Clifford-SU4-SU8, a longer sequence of passes can be required as these circuits consist of a more complicated mixture of gates. In particular, for Clifford-SU4-SU8 the average length of the pass sequence identified by the model is  $\sim 4.36$ . In the case of these two circuit classes, the agent outperforms existing default sequences of passes, suggesting that general purpose passes

agents to assess robustness and avoid bias from selecting a single best-performing run.

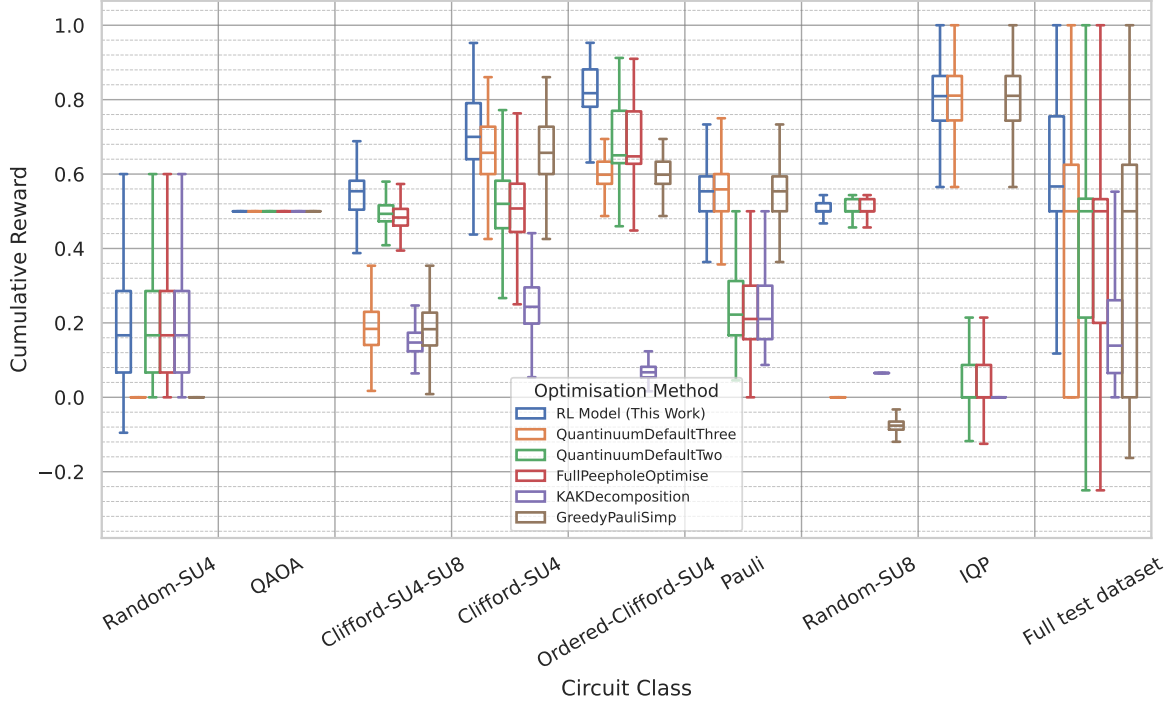


Figure 3: **Cumulative reward (fraction of two-qubit gates removed) for in-distribution circuits.** 40,412 circuits are optimised with nine trained models and a selection of PyTKET optimisation passes. Box plots give the median and interquartile range. Whiskers extend to the the lowest (highest) data point still within 1.5 times the interquartile range of the lower (upper) quartile. ‘Full test dataset’ accumulates all of the circuits.

are not well suited here.

In the case of Ordered-Clifford-SU4 circuits, the order of application of passes is important. In particular, removing the Clifford identities with CliffordSimp or GreedyPauliSimp allows the remaining two-qubit subcircuits to be optimised with KAKDecomposition. The model is almost always (in 99.2% of cases) able to identify this as the correct sequence of passes. Note that neither CliffordSimp or GreedyPauliSimp are the best single first pass to apply, and if only one pass was possible then Three-QubitSquash would perform better. This demonstrates the model’s ability to delay reward in order to select the best sequence of passes.

**Generalisability** Figure 5 compares performance on a test set of 8,115 circuits, roughly equally spread across circuit classes, which are larger than anything in the training set; hence referred to as ‘out-of-distribution’ circuits. Qubit count is in the range [8, 12], and two-qubit gate counts span [216, 450]. As the individual optimisation passes take longer to run on larger circuits, we test with fewer circuits here than for the in-distribution testing, and use just one of the nine trained models. As we do not observe significant variation between seeds, one seed

is chosen at random. We see that performance in Fig. 5 is comparable to that seen in Fig. 3: the (mean, median) fraction of two-qubit gates removed by the agent is (55.7%, 52.0%), compared to (41.5%, 50.0%) for the next best default pass sequence (QuantinuumDefaultThree). This is encouraging, and demonstrates that the model generalises to circuits larger than those seen in the training data. Importantly, this demonstrates that we can deploy the model on large circuits while conducting very manageable training on smaller circuits.

In Fig. 6 we present results from executing our model and the Quantinuum default passes on 1000 very large circuits, with 100 qubits and two-qubit gate counts in the range [878, 1150]. This is at the forefront of qubit counts which can be implemented to date [59]. Again, as executing passes in our action space takes longer with such large circuits, we use fewer than in Fig. 5, but observe similar relative performance between the optimisation passes. The absolute performance is reduced, likely because the circuits are wide and shallow as compared to the circuits used in Figs. 3 and 5.

While Figs. 5 and 6 demonstrate what is possible with our approach, we note that we are limited in this regard by the passes in our action space. Since applying the op-

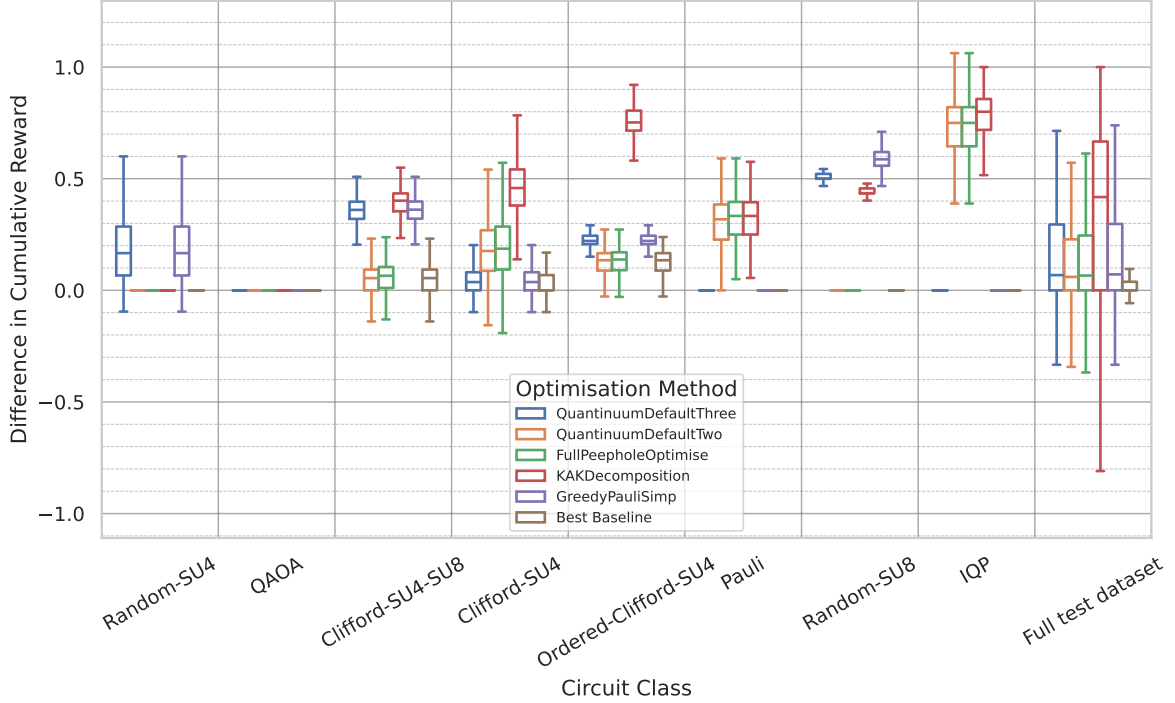


Figure 4: **Difference in cumulative reward (fraction of two-qubit gates removed) between the RL model and baseline optimisation passes for in-distribution circuits.** Positive values indicate improved performance of the RL model. 40,412 circuits are optimised with nine trained models and a selection of PyTKET optimisation methods. Box plots give the median and interquartile range. Whiskers extend to the the lowest (highest) data point still within 1.5 times the interquartile range of the lower (upper) quartile. ‘Full test dataset’ accumulates all of the circuits. ‘Best Baseline’ corresponds to the highest cumulative reward generated by any baseline approach for each circuit.

timisations constitutes the greatest bottleneck, with time to evaluate the model being minimal, improvements to the optimisation passes would increase the reach of our method.

**Scalability** Finally we compare the model to simple beam-search-based optimiser [60, 61]. Beam search is selected as it too generates optimisation-pass sequences bespoke to a given circuit:

**Depth**[ $n$ ]**Width**[ $m$ ]: To construct the search tree, we take the unoptimised circuit to be the root node (level 0). Child nodes are constructed from parents by applying all optimisation passes in the action space, giving one child node per action. At each level of the tree, only a fixed number of nodes (the width,  $m$ ) are retained, with the worst nodes pruned. This is repeated up to a fixed number of levels (the depth,  $n$ ). The best leaf node is returned as the optimised circuit.

**GreedySearch:** Apply each of the optimisation passes in

the action space to the unoptimised circuit, and select the optimised circuit with the lowest two-qubit gate count. This can be thought of as a depth-1 beam search.

**Depth**[ $n$ ]**Width**[ $m$ ] generates a length- $n$  optimisation-pass sequence, while **GreedySearch** generates length-one sequences.

Here we are concerned with exploring the scalability of these approaches to larger circuits and action spaces, and to longer optimisation-pass sequences. As such, we consider circuits in the Clifford-SU4, Ordered-Clifford-SU4, and Clifford-SU4-SU8 circuit classes. These have the most complex structures, and typically require longer optimisation-pass sequences.

In total, we optimise 930 circuits approximately distributed between these three classes; once with each of the search-based optimisation passes, and once with the model. Again, we use only one trained model; i.e. one seed value. Note that we use fewer circuits than in the plots above, to account for the greater runtime of the search-based methods. Qubit counts are in the

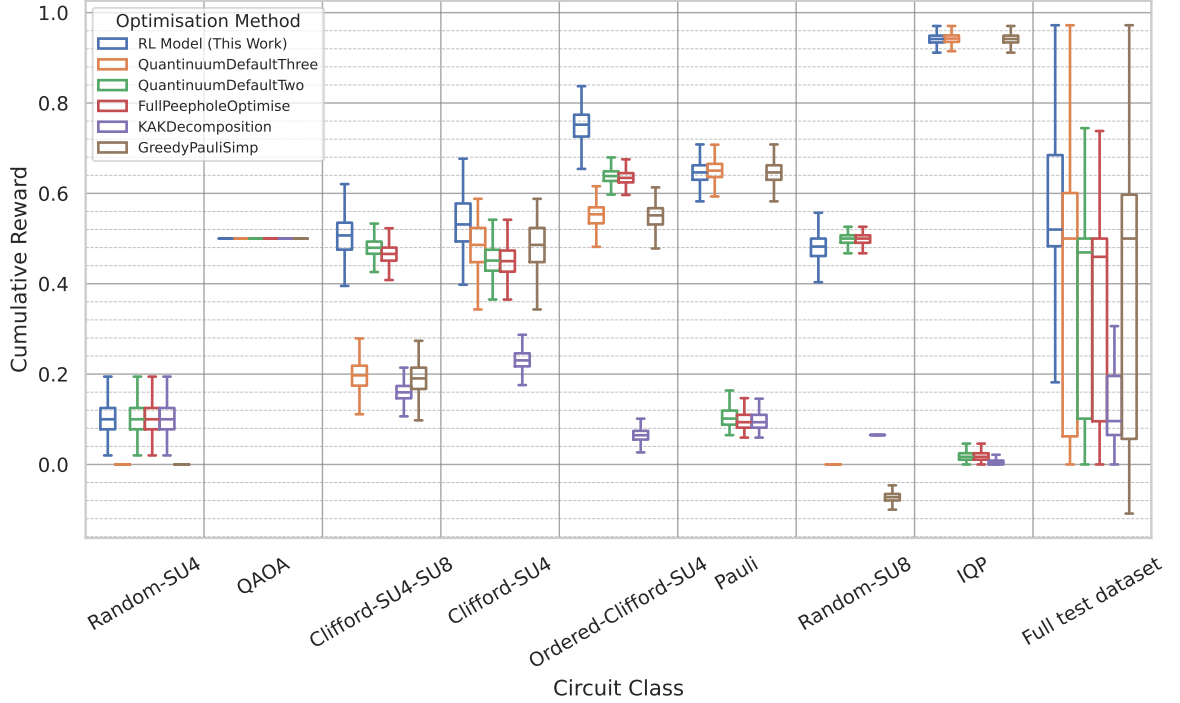


Figure 5: **Cumulative reward (fraction of two-qubit gates removed) for out-of-distribution circuits.** 8,115 circuits are optimised with one trained model and a selection of PyTKET optimisation passes. Box plots give the median and interquartile range. Whiskers extend to the the lowest (highest) data point still within 1.5 times the interquartile range of the lower (upper) quartile. ‘Full test dataset’ accumulates all of the circuits.

range [4, 8], and two-qubit gate counts are in the range [100, 300]. These experiments were conducted on an Apple Macbook Pro with an M3 CPU and 36GB RAM.

Figure 7a demonstrates that the model outperforms GreedySearch and Depth2Width1, and performs comparably to the remaining search-based approaches. However, Fig. 7b shows that the model is notably faster than all of the search-based optimisation methods. This is true even for the very simple GreedySearch, which is comfortably outperformed by our model. We additionally see that the time taken by the model is comparable to QuantinuumDefaultTwo and QuantinuumDefaultThree, although the time taken by the model has a greater spread. This is because the model can select an arbitrary number of passes, while QuantinuumDefaultTwo and QuantinuumDefaultThree apply a fixed number. We see that the beam-search-based approaches improve in performance as the width and depth increases, but that performance plateaus, with the time taken continuing to increase.

This highlights several disadvantages of search-based approaches as compared to our RL-based approach. For a fixed circuit size, the time taken by beam-search-based approaches scales like action space size  $\times$  search width  $\times$  search depth. The time to evaluate the model is mini-

mal compared to the time to execute the action selected. As such, the time taken by our model scales only with the depth. Thus, search-based approaches inevitably scale poorly as the the action space grows. Additionally, when employing search-based approaches it is typically not clear at what level of the search tree to stop. In combination, these pitfalls validate the RL-based approach we have taken here.

It is important to note that for both the model- and search-based optimisers, parallelism can be utilised to decrease the runtime of deployment. We do not consider such improvements in either case in this comparison. Further, as we have discussed, the training time for the model can be notable: 2.73 hours in this case. However, the training need only occur once for the model to then be used as many times as is required. As such, we regard the analysis in this section to be representative of the performance of the model when deployed in practice.

## 5 Conclusion

We have trained an RL agent to generate, given a quantum circuit, a sequence of optimisation passes to best

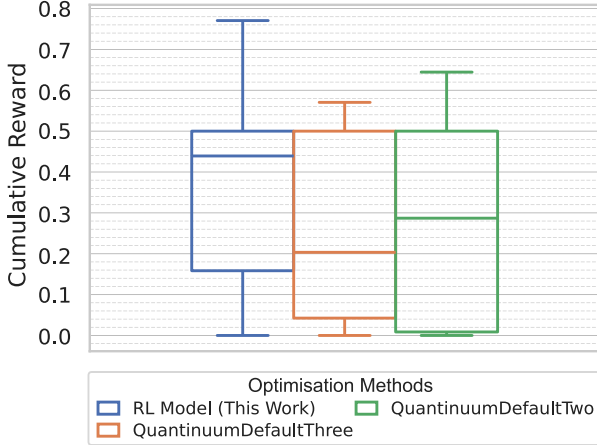
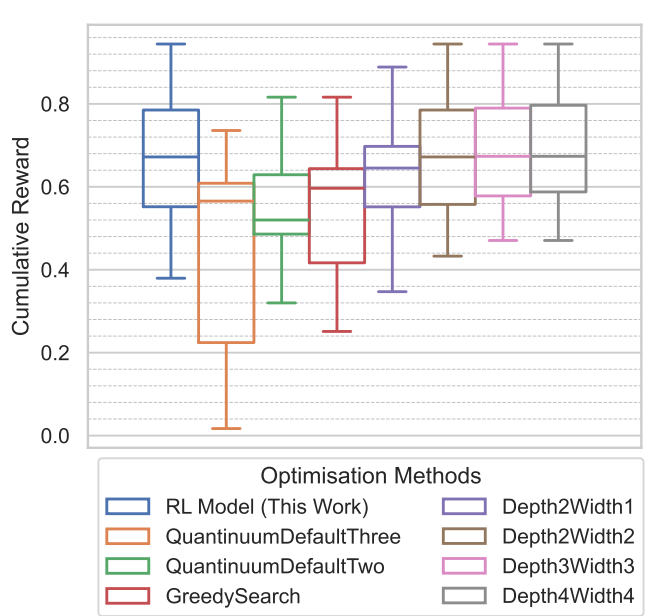


Figure 6: **Cumulative reward (fraction of two-qubit gates removed) for very large out-of-distribution circuits.** 1,000 circuits acting on 100 qubits, equally distributed between all circuit types in Section 3.4, are optimised with one trained model, QuantinuumDefaultTwo, and QuantinuumDefaultThree. Box plots give the median and interquartile range across all circuit types. Whiskers extend to the the lowest (highest) data point still within 1.5 times the interquartile range of the lower (upper) quartile.

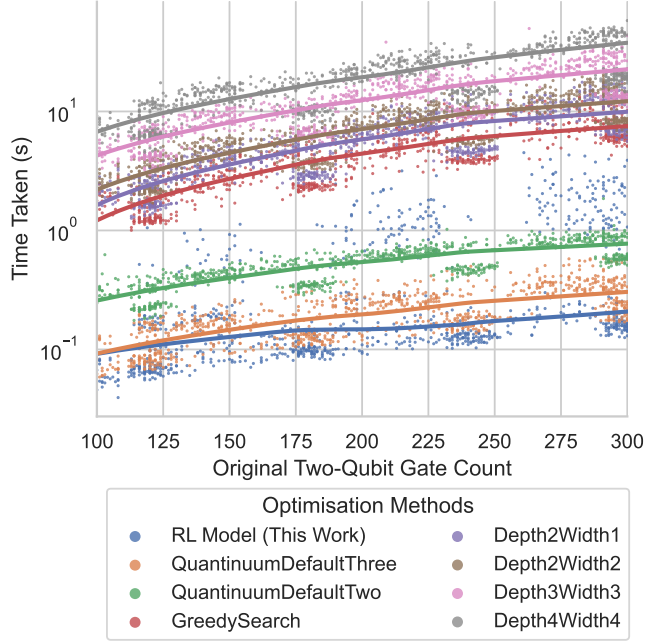
optimise that circuit. The trained agent markedly outperforms default PyTKET optimisation-pass sequences on average over our test set. For each class of circuits in the test set, the agent produces the best – or close to the best – sequence of optimisation passes. We have demonstrated the generalisability of the trained model to circuits larger than anything seen in the training data. We have shown that our RL-based approach is more scalable than other search-based approaches to building bespoke optimisation-pass sequences.

This agent reduces the expertise in quantum circuit compiler theory that is required to orchestrate PyTKET optimisation passes. To make the comparison to default PyTKET optimisation sequences fair, we have limited the action space to PyTKET passes. However, the action space can be straightforwardly expanded to include optimisation passes from other libraries, without any notable changes to the methodology described. We anticipate that an agent trained as described in this paper, but with this expanded action space, will perform better still.

We have demonstrated that bespoke sequences of optimisation passes selected by the model outperform default sequences defined for general use. However using passes which perform global rewrites is still fundamentally limited by the Phase Ordering Problem; passes rewriting the whole circuit may improve the two-qubit gate count in one region of the circuit, but make it worse in another region.



(a) Comparison of cumulative reward (fraction of two-qubit gates removed). Box plots give the distribution across all circuits. Boxes give median and interquartile range, with whiskers extend to the largest/smallest values within 1.5 times the interquartile range.



(b) Comparison of time to optimise. Lines of best fit are a locally weighted scatter-plot smoothing.

Figure 7: **Comparison to search-based optimisation techniques.** A total of 930 circuits from the Clifford-SU4, Ordered-Clifford-SU4, and Clifford-SU4-SU8 circuit classes are optimised for each of the optimisation methods.

A natural application of RL extending the ideas in this paper would be to develop an agent that can select regions of the circuit to rewrite, in addition to selecting the pass to perform on just that region. Note that the region selected may be the whole circuit, combining the benefits of both global and local optimisation.

To further improve the performance of the agent it would be beneficial to expand our training and testing sets to include more circuit types and sizes. In particular, using a training set consisting wholly or partly of real user circuits would be beneficial, although we are not aware of any such sufficiently large training set available at present.

Here we have focused on reducing two-qubit gate count; the dominant noise source for most existing QPUs, and the metric targeted by the majority of optimisation passes available. However, the dominant sources of logical errors when running fault-tolerant circuits may be otherwise; being, for example, T gates when magic state distillation is required [62]. We expect similar techniques to those developed here to be beneficially applied to T-gate count reduction. We encourage investigations of that kind when a notable number of such passes are available.

**Acknowledgements** The authors would like to thank Yao Tang and Matteo Puviani for their careful reviewing of the manuscript. The authors would also like to thank Alan Lawrence, Frederic Rapp, and Stephen Clark for insightful discussions.

## References

- [1] Quantinuum. *Quantinuum H2 Product Data Sheet*. Accessed: 2025-11-01. 2025. URL: [https://docs.quantinuum.com/systems/data\\_sheets/Quantinuum%20H2%20Product%20Data%20Sheet.pdf](https://docs.quantinuum.com/systems/data_sheets/Quantinuum%20H2%20Product%20Data%20Sheet.pdf).
- [2] Seyon Sivarajah et al. “ $t|ket\rangle$ : a retargetable compiler for NISQ devices”. In: *Quantum Science and Technology* 6.1 (Nov. 2020), p. 014003. DOI: 10.1088/2058-9565/ab8e92. URL: <https://dx.doi.org/10.1088/2058-9565/ab8e92>.
- [3] Ali Javadi-Abhari et al. *Quantum computing with Qiskit*. 2024. arXiv: 2405.08810 [quant-ph]. URL: <https://arxiv.org/abs/2405.08810>.
- [4] Ed Younis et al. *Berkeley Quantum Synthesis Toolkit (BQSKit) v1*. [Computer Software] <https://doi.org/10.11578/dc.20210603.2>. Apr. 2021. DOI: 10.11578/dc.20210603.2. URL: <https://doi.org/10.11578/dc.20210603.2>.
- [5] Cirq Developers. *Cirq*. Zenodo, Apr. 2025. DOI: 10.5281/ZENODO.4062499. URL: <https://zenodo.org/doi/10.5281/zenodo.4062499>.
- [6] Robert Wille et al. “The MQT Handbook: A Summary of Design Automation Tools and Software for Quantum Computing”. In: *IEEE International Conference on Quantum Software (QSW)*. 2024. DOI: 10.1109/QSW62656.2024.00013. arXiv: 2405.17543. A live version of this document is available at <https://mqt.readthedocs.io>.
- [7] Aleks Kissinger and John van de Wetering. “PyZX: Large Scale Automated Diagrammatic Reasoning”. In: *Electronic Proceedings in Theoretical Computer Science* 318 (May 2020), pp. 229–241. ISSN: 2075-2180. DOI: 10.4204/eptcs.318.14. URL: <http://dx.doi.org/10.4204/EPTCS.318.14>.
- [8] Jennifer Paykin et al. *PCOAST: A Pauli-based Quantum Circuit Optimization Framework*. 2023. arXiv: 2305.10966 [quant-ph]. URL: <https://arxiv.org/abs/2305.10966>.
- [9] Kesha Hietala et al. “A verified optimizer for Quantum circuits”. In: *Proceedings of the ACM on Programming Languages* 5.POPL (Jan. 2021), pp. 1–29. ISSN: 2475-1421. DOI: 10.1145/3434318. URL: <http://dx.doi.org/10.1145/3434318>.
- [10] Andrew Fagan and Ross Duncan. “Optimising Clifford Circuits with Quantomatic”. In: *Electronic Proceedings in Theoretical Computer Science* 287 (Jan. 2019), pp. 85–105. ISSN: 2075-2180. DOI: 10.4204/eptcs.287.5. URL: <http://dx.doi.org/10.4204/EPTCS.287.5>.
- [11] Cliff Click and Keith D. Cooper. “Combining analyses, combining optimizations”. In: *ACM Trans. Program. Lang. Syst.* 17.2 (Mar. 1995), pp. 181–196. ISSN: 0164-0925. DOI: 10.1145/201059.201061. URL: <https://doi.org/10.1145/201059.201061>.
- [12] John Schulman et al. “Proximal Policy Optimization Algorithms”. In: *CoRR* abs/1707.06347 (2017). arXiv: 1707.06347. URL: <http://arxiv.org/abs/1707.06347>.
- [13] Franco Scarselli et al. “The Graph Neural Network Model”. In: *IEEE Transactions on Neural Networks* 20.1 (2009), pp. 61–80. DOI: 10.1109/TNN.2008.2005605.
- [14] Zonghan Wu et al. “A Comprehensive Survey on Graph Neural Networks”. In: *IEEE Transactions on Neural Networks and Learning Systems* 32.1 (2021), pp. 4–24. DOI: 10.1109/TNNLS.2020.2978386.

[15] Nils Quetschlich, Lukas Burgholzer, and Robert Wille. “Predicting Good Quantum Circuit Compilation Options”. In: *2023 IEEE International Conference on Quantum Software (QSW)*. IEEE, July 2023, pp. 43–53. DOI: 10.1109/qsw59989.2023.00015. URL: <http://dx.doi.org/10.1109/QSW59989.2023.00015>.

[16] Nils Quetschlich, Lukas Burgholzer, and Robert Wille. “Compiler Optimization for Quantum Computing Using Reinforcement Learning”. In: *2023 60th ACM/IEEE Design Automation Conference (DAC)*. IEEE, July 2023, pp. 1–6. DOI: 10.1109/dac56929.2023.10248002. URL: <http://dx.doi.org/10.1109/DAC56929.2023.10248002>.

[17] Nils Quetschlich, Lukas Burgholzer, and Robert Wille. “MQT Predictor: Automatic Device Selection with Device-Specific Circuit Compilation for Quantum Computing”. In: *ACM Transactions on Quantum Computing* 6.1 (Jan. 2025), pp. 1–26. ISSN: 2643-6817. DOI: 10.1145/3673241. URL: <http://dx.doi.org/10.1145/3673241>.

[18] Siddharth Dangwal et al. *Clifford Assisted Optimal Pass Selection for Quantum Transpilation*. 2025. arXiv: 2306.15020 [quant-ph]. URL: <https://arxiv.org/abs/2306.15020>.

[19] Thomas Fösel et al. *Quantum circuit optimization with deep reinforcement learning*. 2021. arXiv: 2103.07585 [quant-ph]. URL: <https://arxiv.org/abs/2103.07585>.

[20] Zikun Li et al. *Quarl: A Learning-Based Quantum Circuit Optimizer*. 2023. arXiv: 2307.10120 [quant-ph]. URL: <https://arxiv.org/abs/2307.10120>.

[21] Maximilian Nägele and Florian Marquardt. “Optimizing ZX-diagrams with deep reinforcement learning”. In: *Machine Learning: Science and Technology* 5.3 (Sept. 2024), p. 035077. ISSN: 2632-2153. DOI: 10.1088/2632-2153/ad76f7. URL: <http://dx.doi.org/10.1088/2632-2153/ad76f7>.

[22] Jordi Riu et al. “Reinforcement Learning Based Quantum Circuit Optimization via ZX-Calculus”. In: *Quantum* 9 (May 2025), p. 1758. ISSN: 2521-327X. DOI: 10.22331/q-2025-05-28-1758. URL: <http://dx.doi.org/10.22331/q-2025-05-28-1758>.

[23] Francois Charton et al. “Teaching small transformers to rewrite ZX diagrams”. In: *The 3rd Workshop on Mathematical Reasoning and AI at NeurIPS’23*. 2023. URL: <https://openreview.net/forum?id=btQ7Bt1NLF>.

[24] Alexander Mattick et al. *Optimizing Quantum Circuits via ZX Diagrams using Reinforcement Learning and Graph Neural Networks*. 2025. arXiv: 2504.03429 [cs.LG]. URL: <https://arxiv.org/abs/2504.03429>.

[25] Mingkuan Xu et al. *Quartz: Superoptimization of Quantum Circuits (Extended Version)*. 2022. arXiv: 2204.09033 [cs.PL]. URL: <https://arxiv.org/abs/2204.09033>.

[26] Amanda Xu et al. “Synthesizing Quantum-Circuit Optimizers”. In: *Proceedings of the ACM on Programming Languages* 7.PLDI (June 2023), pp. 835–859. ISSN: 2475-1421. DOI: 10.1145/3591254. URL: <http://dx.doi.org/10.1145/3591254>.

[27] Francisco J. R. Ruiz et al. *Quantum Circuit Optimization with AlphaTensor*. 2024. arXiv: 2402.14396 [quant-ph]. URL: <https://arxiv.org/abs/2402.14396>.

[28] Alhussein Fawzi et al. “Discovering faster matrix multiplication algorithms with reinforcement learning”. In: *Nature* 610.7930 (Oct. 2022), pp. 47–53. ISSN: 1476-4687. DOI: 10.1038/s41586-022-05172-4. URL: <http://dx.doi.org/10.1038/s41586-022-05172-4>.

[29] Xiangzhen Zhou, Yuan Feng, and Sanjiang Li. “A monte carlo tree search framework for quantum circuit transformation”. In: *Proceedings of the 39th International Conference on Computer-Aided Design*. ICCAD ’20. ACM, Nov. 2020, pp. 1–7. DOI: 10.1145/3400302.3415621. URL: <http://dx.doi.org/10.1145/3400302.3415621>.

[30] Wei Tang et al. *AlphaRouter: Quantum Circuit Routing with Reinforcement Learning and Tree Search*. 2024. arXiv: 2410.05115 [quant-ph]. URL: <https://arxiv.org/abs/2410.05115>.

[31] Matteo G. Pozzi et al. *Using Reinforcement Learning to Perform Qubit Routing in Quantum Compilers*. 2020. arXiv: 2007.15957 [quant-ph]. URL: <https://arxiv.org/abs/2007.15957>.

[32] Alexandru Paler et al. “Machine Learning Optimization of Quantum Circuit Layouts”. In: *ACM Transactions on Quantum Computing* 4.2 (Feb. 2023). DOI: 10.1145/3565271. URL: <https://doi.org/10.1145/3565271>.

[33] Kouhei Nakaji et al. *Quantum circuits as a game: A reinforcement learning agent for quantum compilation and its application to reconfigurable neutral atom arrays*. 2025. arXiv: 2506.05536 [quant-ph]. URL: <https://arxiv.org/abs/2506.05536>.

[34] Yannick Stade et al. *Routing-Aware Placement for Zoned Neutral Atom-based Quantum Computing*. 2025. arXiv: 2505.22715 [quant-ph]. URL: <https://arxiv.org/abs/2505.22715>.

[35] Leo Sünkel et al. *GA4QCO: Genetic Algorithm for Quantum Circuit Optimization*. 2023. arXiv: 2302.01303 [quant-ph]. URL: <https://arxiv.org/abs/2302.01303>.

[36] Mathias Weiden et al. *Improving Quantum Circuit Synthesis with Machine Learning*. 2023. DOI: 10.48550/ARXIV.2306.05622. arXiv: 2306.05622. URL: <https://doi.org/10.48550/arXiv.2306.05622>.

[37] Michael Kölle et al. *A Reinforcement Learning Environment for Directed Quantum Circuit Synthesis*. 2024. arXiv: 2401.07054 [quant-ph]. URL: <https://arxiv.org/abs/2401.07054>.

[38] Mathias Weiden et al. “High-Precision Multi-Qubit Clifford+T Synthesis by Unitary Diagonalization”. In: *Electronic Proceedings in Theoretical Computer Science* 426 (Aug. 2025), pp. 215–230. ISSN: 2075-2180. DOI: 10.4204/eptcs.426.8. URL: <http://dx.doi.org/10.4204/EPTCS.426.8>.

[39] Sebastian Rietsch et al. “Unitary Synthesis of Clifford+T Circuits with Reinforcement Learning”. In: *2024 IEEE International Conference on Quantum Computing and Engineering (QCE)*. IEEE, Sept. 2024, pp. 824–835. DOI: 10.1109/qce60285.2024.00102. URL: <http://dx.doi.org/10.1109/QCE60285.2024.00102>.

[40] Abhishek Sadhu, Aritra Sarkar, and Akash Kundu. “A quantum information theoretic analysis of reinforcement learning-assisted quantum architecture search”. In: *Quantum Machine Intelligence* 6.2 (2024), p. 49.

[41] Antonin Raffin et al. “Stable-Baselines3: Reliable Reinforcement Learning Implementations”. In: *Journal of Machine Learning Research* 22.268 (2021), pp. 1–8. URL: <http://jmlr.org/papers/v22/20-1364.html>.

[42] Robert R. Tucci. *An Introduction to Cartan’s KAK Decomposition for QC Programmers*. 2005. arXiv: quant-ph/0507171 [quant-ph]. URL: <https://arxiv.org/abs/quant-ph/0507171>.

[43] Scott Aaronson and Daniel Gottesman. “Improved simulation of stabilizer circuits”. In: *Physical Review A* 70.5 (Nov. 2004). ISSN: 1094-1622. DOI: 10.1103/physreva.70.052328. URL: <http://dx.doi.org/10.1103/PhysRevA.70.052328>.

[44] Miriam Backens et al. “There and back again: A circuit extraction tale”. In: *Quantum* 5 (Mar. 2021), p. 421. ISSN: 2521-327X. DOI: 10.22331/q-2021-03-25-421. URL: <https://doi.org/10.22331/q-2021-03-25-421>.

[45] Albert T. Schmitz et al. *Graph Optimization Perspective for Low-Depth Trotter-Suzuki Decomposition*. 2023. arXiv: 2103.08602 [quant-ph]. URL: <https://arxiv.org/abs/2103.08602>.

[46] V.V. Shende, S.S. Bullock, and I.L. Markov. “Synthesis of quantum-logic circuits”. In: *IEEE Transactions on Computer-Aided Design of Integrated Circuits and Systems* 25.6 (June 2006), pp. 1000–1010. ISSN: 1937-4151. DOI: 10.1109/tcad.2005.855930. URL: <http://dx.doi.org/10.1109/TCAD.2005.855930>.

[47] Weihua Hu et al. *Strategies for Pre-training Graph Neural Networks*. 2020. arXiv: 1905.12265 [cs.LG]. URL: <https://arxiv.org/abs/1905.12265>.

[48] Kaiming He et al. “Deep Residual Learning for Image Recognition”. In: *CoRR* abs/1512.03385 (2015). arXiv: 1512.03385. URL: <http://arxiv.org/abs/1512.03385>.

[49] Diederik P. Kingma and Jimmy Ba. *Adam: A Method for Stochastic Optimization*. 2017. arXiv: 1412.6980 [cs.LG]. URL: <https://arxiv.org/abs/1412.6980>.

[50] James Bergstra et al. “Algorithms for Hyper-Parameter Optimization”. In: *Advances in Neural Information Processing Systems*. Ed. by J. Shawe-Taylor et al. Vol. 24. Curran Associates, Inc., 2011. URL: [https://proceedings.neurips.cc/paper\\_files/paper/2011/file/86e8f7ab32cf12577bc2619bc635690-Paper.pdf](https://proceedings.neurips.cc/paper_files/paper/2011/file/86e8f7ab32cf12577bc2619bc635690-Paper.pdf).

[51] Andrew W. Cross et al. “Validating quantum computers using randomized model circuits”. In: *Physical Review A* 100.3 (Sept. 2019). ISSN: 2469-9934. DOI: 10.1103/physreva.100.032328. URL: <http://dx.doi.org/10.1103/PhysRevA.100.032328>.

[52] Dan Shepherd and Michael J. Bremner. “Temporally unstructured quantum computation”. In: *Proceedings of the Royal Society A: Mathematical, Physical and Engineering Sciences* 465.2105 (Feb. 2009), pp. 1413–1439. ISSN: 1471-2946. DOI: 10.1098/rspa.2008.0443. URL: <http://dx.doi.org/10.1098/rspa.2008.0443>.

[53] Vojtěch Havlíček et al. “Supervised learning with quantum-enhanced feature spaces”. In: *Nature* 567.7747 (Mar. 2019), pp. 209–212. ISSN: 1476-4687. DOI: 10.1038/s41586-019-0980-2. URL: <http://dx.doi.org/10.1038/s41586-019-0980-2>.

[54] Brian Coyle et al. “The Born supremacy: quantum advantage and training of an Ising Born machine”. In: *npj Quantum Information* 6.1 (July 2020). ISSN: 2056-6387. DOI: 10.1038/s41534-020-00288-9. URL: <http://dx.doi.org/10.1038/s41534-020-00288-9>.

[55] Edward Farhi, Jeffrey Goldstone, and Sam Gutmann. *A Quantum Approximate Optimization Algorithm*. 2014. arXiv: 1411.4028 [quant-ph]. URL: <https://arxiv.org/abs/1411.4028>.

[56] Alexander Cowtan et al. “Phase Gadget Synthesis for Shallow Circuits”. In: *Electronic Proceedings in Theoretical Computer Science* 318 (May 2020), pp. 213–228. ISSN: 2075-2180. DOI: 10.4204/eptcs.318.13. URL: <http://dx.doi.org/10.4204/eptcs.318.13>.

[57] Lightning AI. *Lightning AI — Cloud platform for scalable machine learning*. <https://www.lightning.ai/>. Accessed: 2026-01-19.

[58] Quantinuum. *pytket-quantinuum API Documentation*. Dec. 2025. URL: [https://docs.quantinuum.com/tket/extensions/pytket-quantinuum/api.html#pytket.extensions.quantinuum.backends.quantinuum.QuantinuumBackend.default\\_compilation\\_pass](https://docs.quantinuum.com/tket/extensions/pytket-quantinuum/api.html#pytket.extensions.quantinuum.backends.quantinuum.QuantinuumBackend.default_compilation_pass).

[59] Anthony Ransford et al. *Helios: A 98-qubit trapped-ion quantum computer*. 2025. arXiv: 2511.05465 [quant-ph]. URL: <https://arxiv.org/abs/2511.05465>.

[60] Bruce T. Lowerre. “The Harpy Speech Recognition System”. PhD Thesis. Carnegie Mellon University, 1976.

[61] Peng Si Ow and Thomas E Morton. “Filtered beam search in scheduling”. In: *The International Journal Of Production Research* 26.1 (1988), pp. 35–62.

[62] Sergey Bravyi and Alexei Kitaev. “Universal quantum computation with ideal Clifford gates and noisy ancillas”. In: *Physical Review A* 71.2 (Feb. 2005). ISSN: 1094-1622. DOI: 10.1103/physreva.71.022316. URL: <http://dx.doi.org/10.1103/PhysRevA.71.022316>.